Journal of Power Sources 196 (2011) 1442–1448

Contents lists available at ScienceDirect

Journal of Power Sources

journal homepage: www.elsevier.com/locate/jpowsour

Strain accommodation and potential hysteresis of $LiFePO_4$ cathodes during lithium ion insertion/extraction

Yujie Zhu, Chunsheng Wang*

Department of Chemical & Biomolecular Engineering, University of Maryland, College Park, MD 20742, United States

ARTICLE INFO

Article history:
Received 26 June 2010
Received in revised form 11 August 2010
Accepted 11 August 2010
Available online 19 September 2010

Keywords:
Equilibrium potential hysteresis
Accommodation energy
Galvanostatic intermittent titration Technique
Cycle voltammetry
Electrochemical impedance spectroscopy

ABSTRACT

Equilibrium potential hysteresis of electrode materials refers to the phenomenon that discharge equilibrium potential is lower than charge equilibrium potential. It is induced by the strain accommodation energy of phase transformation. Taking $LiFePO_4$ as an example, the equilibrium potential hysteresis and accommodation energy of two $LiFePO_4$ with different particle sizes were characterized using galvanostatic intermittent titration technique (GITT), cyclic voltammetry (CV), and electrochemical impedance spectroscopy (EIS) methods. The $LiFePO_4$ sample with 40 nm particle size has lower accommodation energy than that of 100 nm $LiFePO_4$, which is due to a narrower miscibility gap and smaller potential hysteresis of 40 nm $LiFePO_4$ comparing to 100 nm $LiFePO_4$. The phase transformation of $LiFePO_4$ occurs only at potential levels above delithiation (charge) equilibrium potential and below lithiation (discharge) equilibrium potential. No phase transformation occurs when charge/discharge is limited in the potential hysteresis range, i.e. $LiFePO_4$ behaves like a solid solution in the potential hysteresis range. A reliable EIS can only be obtained when it is performed at the center of potential hysteresis and the potential amplitude does not exceed the range of equilibrium potential hysteresis. The analysis on strain accommodation and potential hysteresis of $LiFePO_4$ cathodes during Li ion insertion/extraction is also suitable for other phase transformation electrodes.

1. Introduction

$LiFePO_4$ has been considered to be a promising candidate material for the cathode of high-power, safe, low-cost and long-life Li-ion batteries required for hybrid electric vehicles and renewable energy storage. The most striking characteristic of this material is a flat charge/discharge profile at the potential of ~3.4 V versus Li/Li^+ due to the phase transformation. However, pure $LiFePO_4$ suffered from poor rate capability due to low intrinsic electronic/ionic conductivity and slow phase transformation. Extensive research has been carried out to overcome the poor reaction kinetics of $LiFePO_4$. The most effective strategies include (i) to downsize the $LiFePO_4$ particles to nano-scale [1] and (ii) to coat electronically conductive carbon [2] or an ionically conductive phase [3] onto the $LiFePO_4$ particle surface. However, only few studies have been focused on the phase transformation [4–7]. Since most capacity of $LiFePO_4$ comes from a first-order phase transformation, an understanding of the kinetics of the phase transformation is critical to achieving a high-power density for $LiFePO_4$, especially for the carbon-coated nano-$LiFePO_4$ where the electronic and ionic transport have been greatly improved and the slow phase transformation may be a limiting step for the rate performance.

Recent research demonstrated the phase transformation in $LiFePO_4$ is strongly controlled by the strain accommodation energy induced from the volume difference between the lithiated and delithiated phases [4]. The misfit strain between the triphylite phase ($Li_{1-y}FePO_4$) and the heterosite phase (Li_xFePO_4) in nano-$LiFePO_4$ particles was detected using X-ray diffraction (XRD), [4] and dislocations induced by misfit strain were observed in plate-like $LiFePO_4$ particles using transmission electron microscopy (TEM) [8]. Such a strain-induced energy penalty can decrease the driving energy for phase transformation, [9] resulting in decrease of the phase transformation rate [10]. The accommodation energy decreases the lithiation equilibrium potential [9] but increases the delithiation potential, resulting in an equilibrium potential hysteresis [11]. It was reported that shrinking the $LiFePO_4$ particle size can narrow the miscibility gap between the lithiated and delithiated phases and decrease the equilibrium potential hysteresis [4]. The fast phase transformation may be one of the reasons for the excellent rate performance of carbon-coated nano-$LiFePO_4$.

Although the equilibrium potential hysteresis is a critical property of phase transformation electrodes, the characteristics of the equilibrium potential hysteresis of $LiFePO_4$ cathodes have never been investigated. In this paper, the potential hysteresis of

* Corresponding author. Tel.: +1 301 405 0352; fax: +1 301 314 9126.
E-mail address: cswang@umd.edu (C. Wang).

0378-7753/$ – see front matter © 2010 Elsevier B.V. All rights reserved.
doi:10.1016/j.jpowsour.2010.08.008

two $LiFePO_4$ samples with different particle sizes was analyzed using galvanostatic intermittent titration technique (GITT), cyclic voltammetry (CV) and electrochemical impedance spectroscopy (EIS).

2. Experimental methods

Two $LiFePO_4$ samples were provided by a commercial supplier. Transmission electron microscopy (TEM) images for both samples were recorded on a Hitachi HF-2000 FEG-TEM, shown in Fig. 1. The $LiFePO_4$ samples consisted of aggregates of secondary nano-scale crystal particles with average sizes of 40 nm (Fig. 1a) and 100 nm (Fig. 1b). The thin carbon coating (2–4 nm) and crystalline single phases of $LiFePO_4$ can be clearly observed in the high resolution TEM images (Fig. 1c), in which the boundaries between $LiFePO_4$ crystal and carbon coating have been marked. Particle size distributions of two $LiFePO_4$ samples were obtained by randomly measuring 50 particles from the TEM images. The mean particle size of two $LiFePO_4$ samples was calculated by the following equation:

$$d_m = \frac{\sum_i n_i d_i}{\sum_i n_i} \quad (1)$$

where n_i is the number of particles with diameter d_i. Two $LiFePO_4$ samples showed very narrow particle size distribution.

All electrochemical tests in this paper were performed using three-electrode pouch cells. The $LiFePO_4$ cathodes containing 82 wt% active material, 10 wt% carbon black and 8 wt% poly(vinylidesfluoride) (PVDF) in 1-methyl-2-pyrrolidinone (NMP) solvent were prepared by the slurry coating method. The formulation was coated onto aluminum foil with a loading of 2.5 mg cm^{-2} of $LiFePO_4$. The three-electrode pouch cells were assembled in an Ar-filled glove box, using lithium metal as the reference and counter electrodes, 1 M $LiPF_6$ in 1:1:1:3 ethylene carbonate (EC):dimethyl carbonate (DMC):diethyl carbonate (DEC):ethylmethyl carbonate (EMC) as electrolyte and Celgard 3501 as the separator.

To measure the relationship between equilibrium potential (fully relaxed open-circuit-potential (OCP)) and state of charge (SOC) or state of discharge (SOD), cells were tested using a galvanostatic intermittent titration technique (GITT). All the GITT tests have been performed using *Arbin* test station. GITT measurements consisting of a series of current pulses were applied to the three-electrode pouch cells at a low current of less than 0.022 C for 2 h, each followed by a 16 h rest process. The OCP at the end of the 16th hour is considered to be the equilibrium potential. The potential decay during the rest process includes both relaxation and self-discharge. $LiFePO_4$ electrodes cannot be fully relaxed to equilibrium if the relaxation time is too short. However, a relaxation time that is too long will greatly increase the testing time, resulting in noticeable self-discharge. The potential decay will be mainly controlled by self-discharge if relaxation time is much longer than 16 h, as evidenced from the capacity difference between charge GITT and discharge GITT. The relaxation time of 16 h was selected to allow full relaxation of OCP and to minimize the self-discharge of $LiFePO_4$ during the test. The potentials of 2.2 and 4.2 V were used as the low and high cutoff voltages in GITT tests.

To characterize the equilibrium potential hysteresis of $LiFePO_4$ in the phase transformation region, cyclic voltammetry (CV) at a scan rate of 0.05 mV s^{-1} was performed on electrodes at the middle of potential hysteresis between 50% SOC and 50% SOD using different scan potential amplitudes. A low scan rate of 0.05 mV s^{-1} is used here to decrease the influence of lithium ion diffusion on the current but detect the phase transformation current [12]. Similarly, electrochemical impedance spectroscopy (EIS) was also applied on the $LiFePO_4$ cathodes at 50% SOC, 50% SOD and at the middle of potential hysteresis between 50% SOC and 50% SOD. Before CV and EIS tests, the electrodes were charged/discharged between 2.2 and 4.2 V at 0.1 C current for two cycles. Both CV and EIS were tested on Solartron 1260/1287.

3. Results and discussion

3.1. Equilibrium potential hysteresis of $LiFePO_4$ induced by accommodation energy

Delithiation/lithiation of $LiFePO_4$ is usually accompanied by phase transformation between heterosite phase (α phase) and triphylite phase (β phase) [4]. The formation of potential hysteresis during delithiation and lithiation of $LiFePO_4$ was discussed in our publication [13]. In brief, during Li ion insertion, the lattice parameters of the Li_xFePO_4 vary with the lithium stoichiometry and phase transformation, since the newly formed phase has a different molar volume with that of the matrix [4,14]. To accommodate the volume difference, stress and strain will be generated during Li ion insertion into $FePO_4$. For a purely elastic matrix, elastic energy will be stored in the matrix and the newly formed phase during phase transformation [15]. For a plastic matrix with a low yield strength, the elastic energy stored in the matrix will be relaxed and spent in creating plastic deformation [16]. Normally, the electrode materials are elastic–plastic solid, the transformation energy is accommodated by both elastic and plastic energy [15]. The plastic deformation in $LiFePO_4$ during phase transformation has been evidenced from the existence of dislocations and fracture [8,17]. The elastic–plastic accommodation energy is an energy barrier against lithiation and delithiation [9]. It increases the free energy of the material and decreases the lithiation equilibrium potential. The decrease of lithiation equilibrium (open-circuit) potential $\Delta E_{lithiation}$ can be determined from [15,18].

$$\Delta E_{lithiation} = E_o - E_{de} = \frac{\Delta G^{elastic}_{lithiation} + \Delta G^{plastic}_{lithiation}}{nF} \quad (2)$$

where E_o is the theoretical (*accommodation-free*) equilibrium potential, E_{de} is the discharge equilibrium potential after consideration of the accommodation process during Li ion insertion, $\Delta G^{elastic}_{lithiation}$ and $\Delta G^{plastic}_{lithiation}$ are elastic and plastic accommodation energy during lithiation process, n is the number of electrons passed per atom of host material reacted and F is the Faraday's constant. The accommodation energy increases with the depth of discharge process, which is similar to the strain-hardening phenomenon observed in phase transformation of metal hydrides [19].

During Li ion extraction, a reverse phase transformation will occur. The volume changes during the Li ion extraction will also be accommodated by the elastic–plastic process outlined above. Different from the lithiation process, the accommodation energy during Li ion extraction increases the electrode potential. The potential increase during the charge (delithiation) process can be calculated as

$$\Delta E_{delithiation} = E_{ce} - E_o = \frac{\Delta G^{elastic}_{delithiation} + \Delta G^{plastic}_{delithiation}}{nF} \quad (3)$$

where E_{ce} is the charge equilibrium potential after consideration of the accommodation process, $\Delta G^{elastic}_{delithiation}$ and $\Delta G^{plastic}_{delithiation}$ are elastic and plastic accommodation energy during delithiation process. The accommodation processes during Li ion insertion and extraction dissipate energy to the surroundings, resulting in an open-circuit-potential hysteresis ($\Delta E_{lithiation} + \Delta E_{delithiation}$). Therefore, the equilibrium (open-circuit) potential hysteresis during Li ion insertion and extraction can be calculated from the accommodation energy. From the accommodation energy of Li–Sn alloy, Hirai et al. [9] calculated the lithiation equilibrium potential of Sn using Eq. (2), which is in excellent agreement with measured data. Eqs. (2)

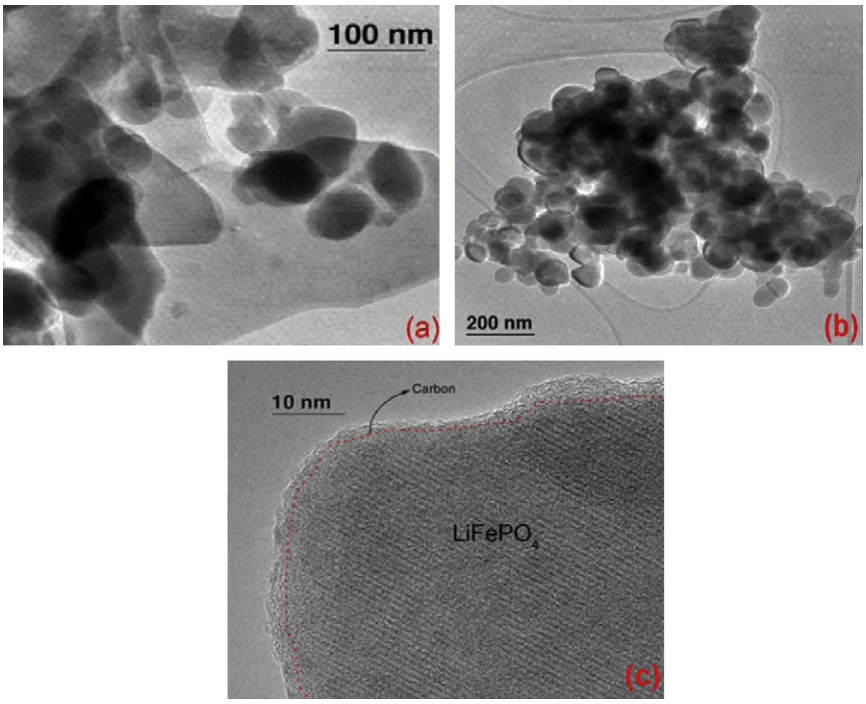

Fig. 1. TEM images for (a) $LiFePO_4$ with secondary particle size ~40 nm and (b) $LiFePO_4$ with secondary particle size ~100 nm. (c) The carbon coating layer on a crystal $LiFePO_4$ particle is marked in HTEM.

and (3) have also been applied in the metal–hydrogen system for determining the pressure hysteresis of metal hydrides from their accommodation energy [11].

Equilibrium potential hysteresis of phase transformation electrode during lithiation and delithiation can easily be determined using GITT, however, the accommodation energy is very difficult to obtain from materials properties especially for new electrode materials. Based on the relationship between potential hysteresis and accommodation energy in Eqs. (2) and (3), the accommodation energy can be calculated from equilibrium potential hysteresis.

The following reaction occurs during phase transformation from heterosite (Li_xFePO_4) to triphylite ($Li_{1-y}FePO_4$).

$$Li_xFePO_4 + (1-y-x)Li^+ + (1-y-x)e^- \underset{delithiation}{\overset{lithiation}{\rightleftarrows}} Li_{1-y}FePO_4 \quad (4)$$

When the accommodation energy ($\Delta G^{accomm}_{lithiation} = \Delta G^{elastic}_{lithiation} + \Delta G^{plastic}_{lithiation}$) change during lithiation is defined as *joules per molar of FePO4*, the accommodation energy for the lithiation process can be expressed as

$$\Delta G^{accomm}_{lithiation} = (1-x-y)F\Delta E_{lithiation} \quad (5)$$

Since the values of x, $1-y$ and $\Delta E_{lithiation}$ can be obtained from the equilibrium potential-composition isotherm curves, [15] the accommodation energy can be calculated using Eq. (4). Similarly, the accommodation energy during delithiation can also be obtained using

$$\Delta G^{accomm}_{delithiation} = (1-x-y)F\Delta E_{delithiation} \quad (6)$$

The equilibrium potential of $LiFePO_4$ with secondary particle sizes of 40 and 100 nm were tested at different levels of lithiation and delithiation (Fig. 2). The equilibrium potentials of both $LiFePO_4$ electrodes gradually decreased with Li ion insertion but increased with Li ion extraction. The variation in equilibrium potential of 40 nm $LiFePO_4$ during Li ion insertion and extraction is less than that of 100 nm $LiFePO_4$. Both $LiFePO_4$ particles have a similar delithiation equilibrium potential within the miscibility gap, however, the lithiation equilibrium potential of 40 nm $LiFePO_4$ is 5–6 mV higher than that of 100 nm $LiFePO_4$, resulting in a smaller potential hysteresis (8–10 mV) for 40 nm $LiFePO_4$, compared to 13–16 mV for 100 nm $LiFePO_4$. In addition, nano-scale (40 nm) $LiFePO_4$ has a reduced miscibility gap compared to coarser-grained (100 nm) materials. The size-dependent potential hysteresis and miscibility gap shown in Fig. 2 are well in agreement with the observations from other researchers [4,5,20].

The accommodation energies of $LiFePO_4$ with different particle sizes during the first cycle of lithiation and delithiation in the phase transformation region were calculated from equilibrium potential hysteresis using Eqs. (5) and (6) and shown in Fig. 3. The theoretical equilibrium potential E_o is defined as the average value of potentials, at which the charge and discharge phase transformation

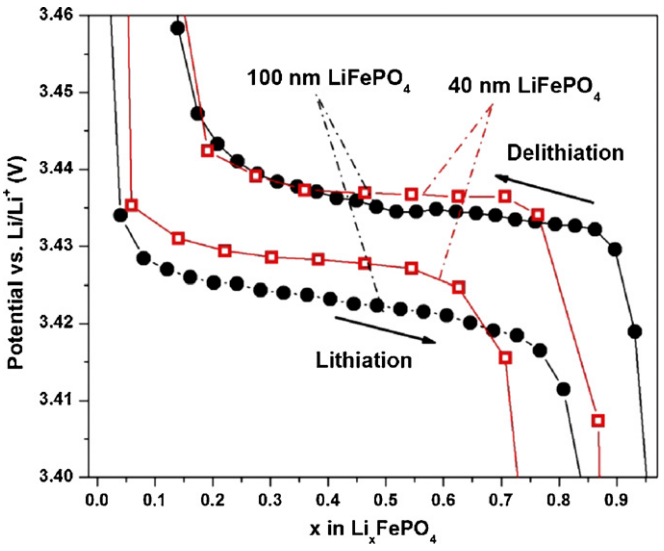

Fig. 2. GITT equilibrium potential for $LiFePO_4$ with different particle sizes.

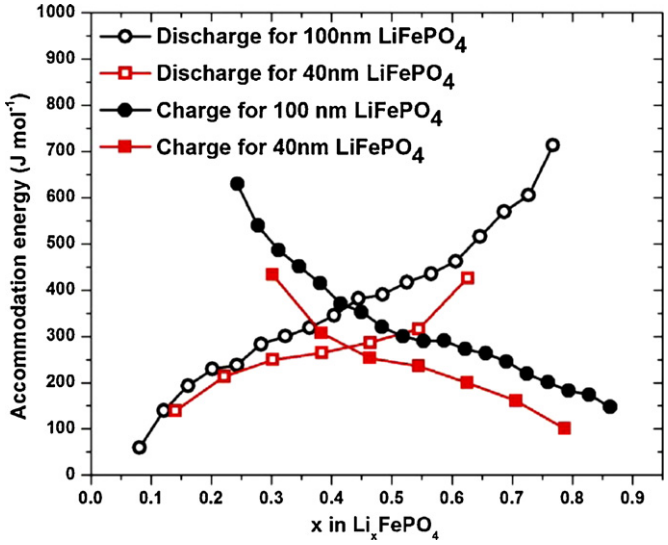

Fig. 3. Discharge and charge accommodation energy for $LiFePO_4$ with different particle sizes.

initiated. Compared to 100 nm $LiFePO_4$, 40 nm $LiFePO_4$ has a lower accommodation energy due to a narrow potential hysteresis and a reduced miscibility gap in nano-size $LiFePO_4$ [5]. Both the short diffusion length and a low accommodation energy in nano-$LiFePO_4$ accelerate the phase transformation rate, resulting in high rate performance [4]. The accommodation energy of both $LiFePO_4$ samples increased with SOD and SOC. At $Li_{0.5}FePO_4$, the discharge (lithiation) accommodation energy is larger than the charge (delithiation) accommodation energy. The reduced accommodation energy in charge compared to discharge may be one of the reasons for higher charge rate capability of $LiFePO_4$ than that for discharge [21].

It has been reported that dislocations and other defects were generated during the first cycle of Li ion insertion/extraction in $LiFePO_4$ [8,17]. These defects change the accommodation energy in the following cycles. Therefore, the accommodation energy in the second charge/discharge cycle may be different from the values in the first cycle. Fig. 4a compares the equilibrium potentials of 100 nm $LiFePO_4$ in the first and second charge/discharge cycles. The corresponding accommodation energies in the first and second charge and discharge cycles are illustrated in Fig. 4b. As shown in Fig. 4a, the discharge equilibrium potential in the second charge/discharge cycle is almost the same as that in the first cycle, but the charge equilibrium potential in the second charge/discharge cycle is lower than that in the first cycle at later SOC. The lower charge equilibrium potential induced lower charge accommodation energy in the second charge cycle. These behaviors are most likely due to (i) the introduction of dislocations and/or fractures in micro-$LiFePO_4$ in the first charge/discharge cycle, which lowered the energy required for phase growth for the second charge cycle, and (ii) the volume expansion/shrinkage of $LiFePO_4$ during the first charge/discharge cycle, which may locally rearrange the position of $LiFePO_4$ particles to accommodate the stress. The reduced accommodation energy during the initial charge/discharge cycles is consistent with the activation process of $LiFePO_4$ electrodes. However, why these defects only affect the charge accommodation energy but not the discharge accommodation energy is not clear.

As shown in Fig. 4b, the discharge accommodation energy of 100 nm $LiFePO_4$ increased up to 750 J mol^{-1} when Li_xFePO_4 (α phase) gradually transformed into $Li_{1-y}FePO_4$ (β phase). The maximum accommodation energy (750 J mol^{-1}) of $LiFePO_4$ during phase transformation from Li_xFePO_4 to $Li_{1-y}FePO_4$ is less than the accommodation energy (972 J mol^{-1}) of Nb during phase transformation

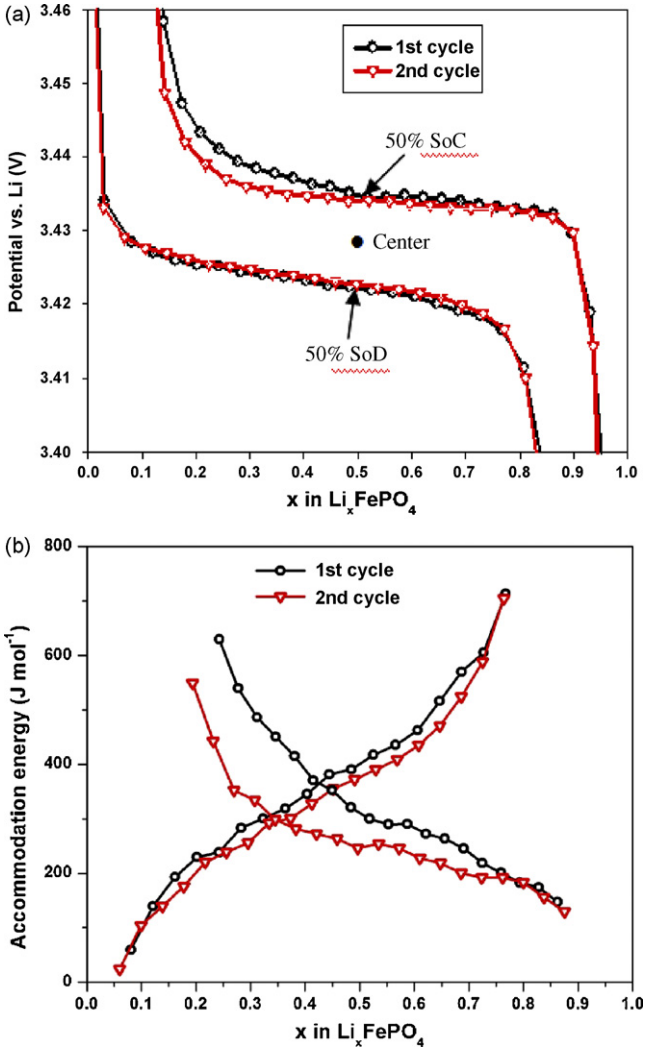

Fig. 4. (a) GITT equilibrium potential at different cycles and (b) charge and discharge accommodation energy at different cycles.

from Nb to NbH [15] and is much smaller than the accommodation energy (9630 J mol^{-1}) of Sn during phase transformation from Sn to $Li_{0.4}Sn$ [9]. Therefore, the exceptional rate performance of $LiFePO_4$ may be partially attributed to the lower accommodation energy during phase transformation compared to Sn anode for Li-ion battery and Nb–hydride anodes for Ni/MH batteries.

3.2. Characterization of potential hysteresis with GITT

To characterize the property of equilibrium potential hysteresis of $LiFePO_4$, the delithiation equilibrium potential of 100 nm $LiFePO_4$ was measured after being equilibriately discharged to different levels (SOD: 40%, 60%, 80% and 100%) using GITT and shown in Fig. 5. At a given Li ion concentration, the charge equilibrium potential increased with the depth of the previous SOD. For example, the electrode with composition $Li_{0.3}FePO_4$, which was previously completely discharged, has the highest charge equilibrium potential, while the $Li_{0.3}FePO_4$ electrode that was previously discharged to $Li_{0.4}FePO_4$ has the lowest charge equilibrium potential. Although the equilibrium potential of the following charge process increased with the depth of previous SOD, the initial potential for the phase transformation from β to α phase during charge process occurs at the same value (see A–B line in Fig. 5) no matter how much Li ion was inserted into $FePO_4$ in the previous discharge. If the

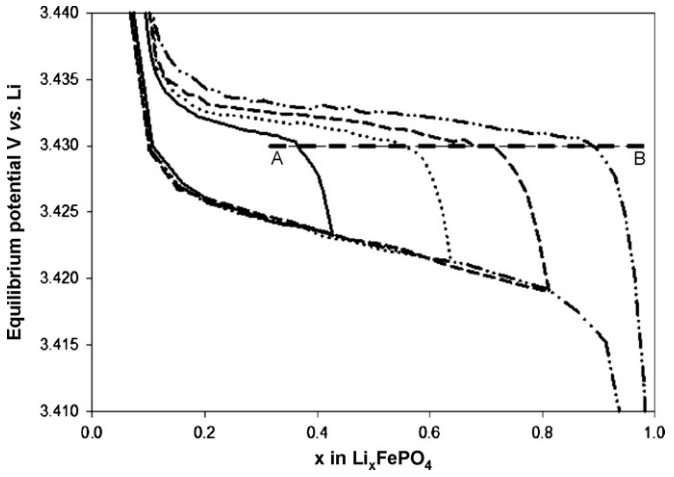

Fig. 5. Charge equilibrium potential of 100 nm $LiFePO_4$ following SOD 40%, 60%, 80, and 100%. Discharge and charge current: 0.022 C, discharge time: 2 h, charge time: 0.33 h for 40% and 0.67 h for 60, 80 and 100%. Rest time for charge and discharge: 8 h.

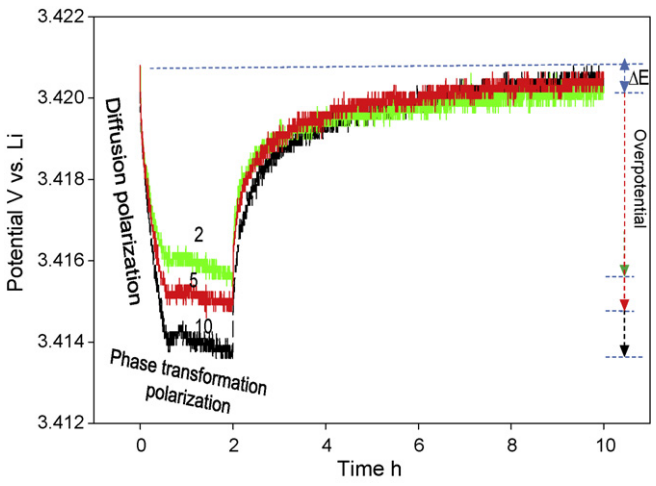

Fig. 7. Discharge and following rest potential during GITT at the 2nd, 5th and 10th current pulses.

charge equilibrium potential lines previously discharged to SOD 40%, 60% and 80% are moved along the A → B direction to the charge potential line previously discharged to SOD 100%, four charge lines will be completely overlapped. Therefore, the charge equilibrium potentials following different SOD levels are solely attributed to the fraction of newly formed α phase rather than the fraction of α phase left during previous SOD.

To illustrate the kinetics of charge and discharge of $LiFePO_4$, the potential responses during each current pulse in the GITT measurement were recorded and shown in Fig. 6. Due to the resolution limitation of *Arbin* equipment, the potential jump due to solid-electrolyte-interphase resistance and charge transfer reaction cannot be monitored. The polarization curves recorded in Fig. 6 only reflect potential change due to Li-ion diffusion and the phase transformation. As demonstrated in Fig. 6, both charge and discharge overpotentials increased with the fraction of new phase. To investigate the kinetics of discharge at different SOD, the GITT potential-time profiles at the 2nd, 5th and 10th discharge pulse were compared by shifting their initial open-circuit potentials together, as shown in Fig. 7. The changes in equilibrium OCP (ΔE in Fig. 7) before and after current pulses are almost the same in three current pulses. However, overpotential (the potential difference between fully relaxed OCP and the potential at the end of the current pulse) in Fig. 7 increased with SOD. By carefully comparing the potential response in each current pulse (Fig. 7), we found that the initial potential exponentially drops, followed by an almost linear decrease with time. The initial potential drop is due to the Li-ion diffusion, and the later slow decrease in potential is attributed to the phase transformation. The diffusion polarization quickly increases with SOD, but the phase transformation polarization only slightly changes with SOD. Fig. 7 demonstrates that the increase in overpotential with SOD is mainly attributed to the increase in Li-ion diffusion length due to the growth of the β phase. The increase in diffusion overpotential with phase transformation was also observed in the lithiation/delithiation of graphite [22].

The charge GITT following different SOD was used to characterize potential hysteresis. As shown in Fig. 6 the polarization curves are SOD-independent, i.e. the potential responses in charge GITT following different SOD were similar at the same potential level except for 40% SOD in which the charge time of $LiFePO_4$ was shortened from 0.66 h (for all other SOD) to 0.33 h to get more equilibrium potential data. To clearly show the potential response, the discharge and charge GITT curves at 60% SOD were enlarged and shown in Fig. 8. The potential response in each charge GITT curve shows only exponential increase (diffusion polarization) without linear polarization (phase transformation polarization) until the 7th charge GITT curve, where the polarization potential exceeds the charge equilibrium potential and phase transformation occurs. Therefore, no phase transformation occurs inside potential hys-

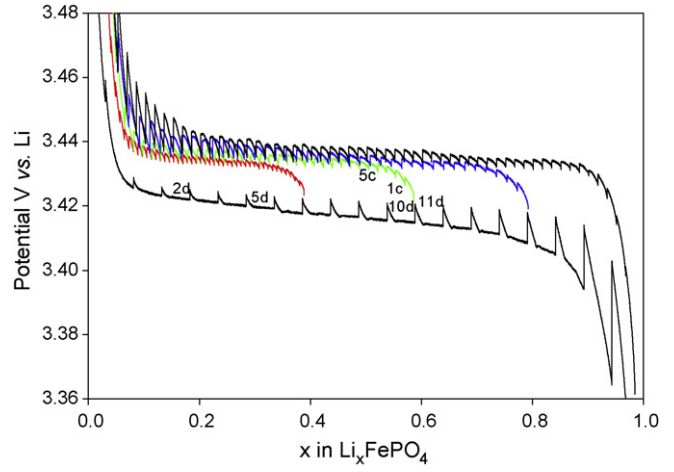

Fig. 6. Charge GITT curves following different SOD.

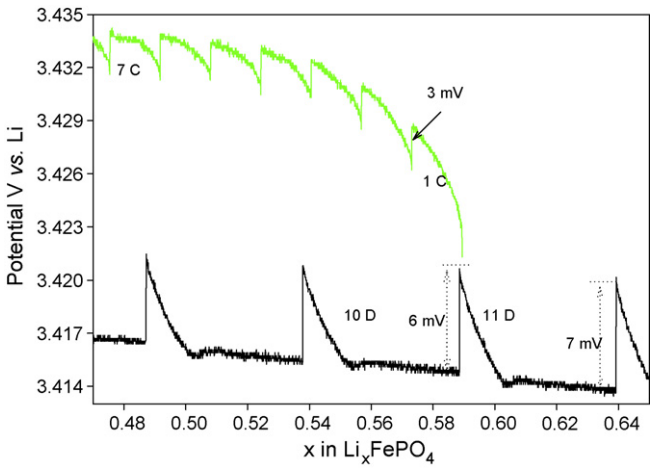

Fig. 8. Charge and discharge GITT at 60% SOD.

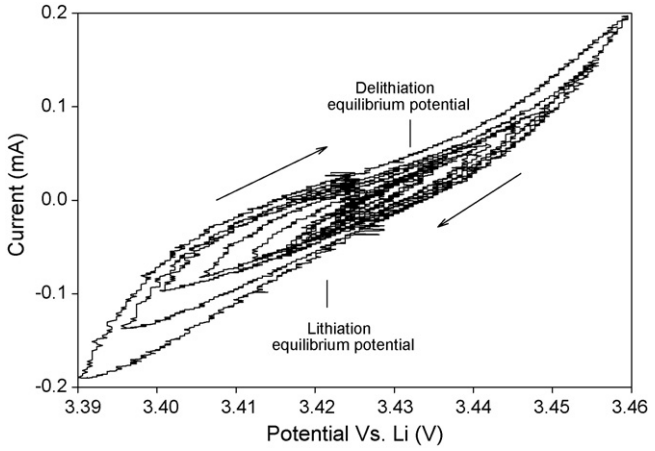

Fig. 9. CV performed at the middle of voltage hysteresis with different amplitudes.

teresis region. Although in the potential hysteresis region, $LiFePO_4$ still consists of two phases, it behaves like a solid solution. Here, we need to point out that during charge/discharge, in the potential hysteresis region, Li ions can penetrate across the interface, and the interface between two phases in $LiFePO_4$ does not move, which is different from the behavior of phase transformation and similar to solid solution. The solid solution behavior in the potential hysteresis region is also supported by the fact that the charge polarization curves after different SOD are similar to the charge polarization curves after fully discharged (100% SOD), shown in Fig. 6, and the fully discharged (100% SOD) $LiFePO_4$ is a solid solution before the charge potential reaches the charge equilibrium potential. In addition, the first charge overpotential is much smaller than the previous discharge overpotentials. For example, the overpotential at the 10th discharge GITT (10d in Fig. 8) is around 6.0 mV at the discharge current of 0.022 C. However, the overpotential in the first charge GITT (1c in Fig. 8) is only 3 mV at the same current, while the overpotential in the following discharge GITT (11d in Fig. 8) is 7 mV. The difference between the 11th discharge and the 1st charge is that phase transformation occurs in the 11th discharge, while no phase transformation takes place in the 1st charge. The phase transformation overpotential at the 11th discharge GITT is around 4.0 mV, which is 57% of the total (phase transformation and diffusion) overpotential.

3.3. Characterization of phase transformation potential hysteresis with CV and EIS

Cycle voltammetry (CV) is a common and useful tool to distinguish the phase transformation from a solid solution because the current will be enhanced in the phase transformation region. Therefore, the CV is used to characterize the phase transformation behavior of $LiFePO_4$ across the potential hysteresis where the phase transformation of $LiFePO_4$ occurs only when the applied potential is lower than the lithiation equilibrium potential or higher than delithiation equilibrium potential. $LiFePO_4$ in the potential hysteresis range can be considered as a solid solution material. Fig. 9 shows the CV scans of 100 nm $LiFePO_4$ at the center of potential hysteresis (marked in Fig. 4a) using different scan potential amplitudes but a fixed scan rate of 0.05 mV s^{-1}. Before each CV measurement, the 100 nm $LiFePO_4$ electrode was fully charged to 4.2 V and then discharged to SOD 50% followed by charging the electrode to 3.427 V and holding the electrode at this potential for 2 h. 3.427 V is the potential halfway between lithiation potential (3.422 V) and delithiation potential (3.432 V). By changing the amplitude of CV (±2, ±4, ±6, ±8, ±10, ±12, ±15, ±20, ±25, ±30, ±35 mV), the reversibility of the reactions inside and outside of the

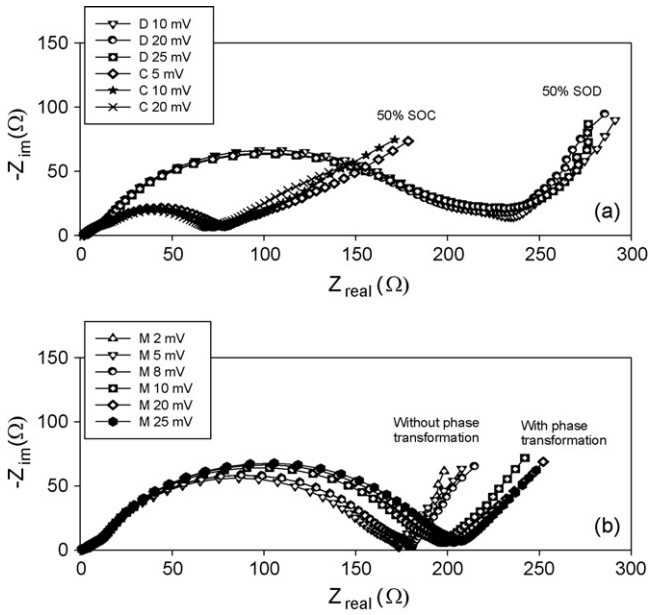

Fig. 10. EIS plots measured at (a) OCP of 50% SOD and 50% SOC, and (b) the middle potential of the potential hysteresis with different voltage amplitudes.

potential hysteresis range was characterized. When the amplitudes of CV are similar or less than the half value of potential hysteresis (6–8 mV), the potential almost linearly changed with current. However, for CV with a large amplitude (>12 mV), a rapid increase in current was observed when the lithiation potential was below 3.42 V and delithiation potential was above 3.435 V, which is due to the phase transformation. The CV scans starting at the center of potential hysteresis with different potential amplitudes demonstrated solid solution behavior inside the potential hysteresis and phase transformation characteristic outside of the potential hysteresis range.

EIS has been widely used in Li-ion batteries to evaluate the charge/discharge kinetics. A reliable EIS can be obtained only if the system satisfies the criteria of linearity and time invariance (LTI) [23]. If EIS is measured at the open-circuit after charging or discharging to a given state, the phase transformation occurs only in the forward potential scan, not in the backward potential scan, resulting in a SOD or SOC shift during EIS measurement. Therefore, the $LiFePO_4$ is not a linear and time invariant system if EIS is measured at the certain charge or discharge equilibrium potentials. The EIS normally measured at different SOD or SOC are not reliable. A reliable and useful EIS can only be obtained by shifting the testing potential to the center of the potential hysteresis. Fig. 10 shows the EIS plots measured at 50% SOD, 50% SOC and in the center of the potential hysteresis (marked in Fig. 4a) with different potential amplitudes. To alleviate OCP shift during the EIS measurement, the $LiFePO_4$ sample after each EIS measurement at 50% SOD (or 50% SOC) was fully re-charged (or fully re-discharged for SOC) and then discharged to 50% SOD (or charged to 50% SOC) for the following EIS test. The impedances of $LiFePO_4$ in Fig. 10 consist of two semicircles and a sloped line. For a solid solution electrode, the high frequency semicircle in EIS is attributed to the SEI film, middle frequency semicircle to charge transfer, and low frequency line to diffusion. The impedance at 50% SOC is much smaller than that at 50% SOD, resulting in higher rate capability in charge than in discharge. EIS in both 50% SOD and 50% SOC are less sensitive to signal amplitude.

Since the EIS performed at charge or discharge equilibrium potential is not reliable, EIS should be performed at the center of potential hysteresis. When the EIS test is conducted at the cen-

ter of potential hysteresis using amplitudes less than half of the potential hysteresis, the $LiFePO_4$ can be treated as a solid solution since no phase transformation occurs in the potential hysteresis region. When the amplitude of EIS test is much larger than half of the potential hysteresis, the phase transformation can happen. In this case, if the kinetics of forward phase transformation is similar to the backward phase transformation, a reliable EIS can still be obtained. The EIS measured at the center of potential hysteresis using different amplitudes was shown in Fig. 10. The impedances with amplitudes larger than half of the potential hysteresis have a larger second semicircle than those with amplitudes less than the potential hysteresis, which indicate that phase transformations cause additional impedance. The phase transformation impedance appears at a higher frequency than Li-ion diffusion impedance and is mixed with the impedance of the charge transfer reaction. The phase transformation impedance of $LiFePO_4$ was obtained by subtracting impedance without phase transformation from phase transformation impedance. The phase transformation impedance of $LiFePO_4$ is around 20 Ω. The phase transformation impedance is 50% of total (phase transformation + ion diffusion) impedance, which is similar to the overpotential ratio (57%) obtained using GITT in Fig. 8.

4. Conclusions

Equilibrium potential hysteresis of $LiFePO_4$ is a thermodynamic property, which is induced by strain accommodation energy. The OCP hysteresis of $LiFePO_4$ in the phase transformation region was determined using the GITT method, and the corresponding accommodation energies were calculated according to the potential hysteresis. 40 nm-$LiFePO_4$ has low accommodation energy during lithiation and delithiation, which is attributed to the narrow miscibility gap and small potential hysteresis. Phase transformation only occurs at a potential level above charge OCP or below discharge OCP. The $LiFePO_4$ inside potential hysteresis region behaves like a solid solution. Normal EIS obtained at different SOD or SOC cannot satisfy the criteria of linearity and time invariance (LTI). A reliable EIS can be obtained at the center of potential hysteresis, and phase transformation impedance can be obtained by changing the amplitude of the EIS signal from less than to greater than half of the potential hysteresis.

Acknowledgement

The authors gratefully acknowledge the support of the National Science Foundation under Contract No. CBET0933228 (Dr. Maria Burka, Program Director).

References

[1] N. Meethong, H.S. Huang, W.C. Carter, Y.M. Chiang, Electrochem. Solid-State Lett. 10 (2007) A134.
[2] M.M. Doeff, F. Hu, F. Mclarnon, R. Kostecki, Electrochem. Solid-State Lett. 6 (2003) A207.
[3] O. Kang, G. Ceder, Nature 458 (2009) 190.
[4] N. Meethong, H.S. Huang, S.A. Speakman, W.C. Cater, Y.M. Chiang, Adv. Funct. Mater. 17 (7) (2007) 1115.
[5] N. Meethong, Y.H. Kao, M. Tang, H.Y. Huang, W.C. Carter, Y.M. Chiang, Chem. Mater. 20 (2008) 6189–6198.
[6] C. Delmas, M. Maccario, L. Croguennec, F.L. Cras, F. Well, Nat. Mat. 7 (2008) 665.
[7] G. Kobayashi, S.I. Nishimura, M.S. Park, R. Kanno, M. Yashima, T. Ida, A. Yamada, Adv. Funct. Mater. 19 (7) (2009) 395.
[8] H. Gabrisch, J. Wilcox, M.M. Doeff, Electrochem. Solid-State Lett. 11 (2008) A25.
[9] K. Hirai, T. Ichistubo, T. Uda, A. Miyazaki, S. Yagi, E. Matsubara, Acta Mater. 56 (2008) 1539.
[10] E. Gamsjager, T. Antretter, C. Schmaranzer, W. Preis, C.M. Chimani, N.K. Simha, J. Svoboda, F.D. Fischer, Comput. Mater. Sci. 25 (2002) 92–99.
[11] R. Balasubramaniam, J. Alloys Compd. 253 (1997) 203.
[12] M.D. Levi, D. Aurbach, J. Phys. Chem. B 101 (1997) 4630.
[13] Y. Zhu, C. Wang, J. Phys. Chem. C 114 (2010) 2830–2841.
[14] S.I. Pyun, J.Y. Go, T.S. Jang, Electrochim. Acta 49 (2004) 4477.
[15] R. Balasubramaniam, Acta Metall. Mater. 41 (1993) 3341.
[16] H.K. Bimbaum, M.L. Grossbeck, M. Amano, J. Less-common Metals 49 (1976) 357.
[17] G. Chen, X. Song, T.J. Richardson, Electrochem. Solid-State Lett. 9 (2006) A295.
[18] C.R. Krenn, Model. Simul. Mater. Sci. Eng. 12 (2004) S415.
[19] Y.Y. Earmme, W.C. Johnson, J.K. Lee, Metall. Trans. A 2 (1981) 1521.
[20] K.T. Lee, W.H. Kan, L.F. Nazar, J. Am. Chem. Soc. 131 (2009) 6044.
[21] V. Srinivasan, Newman, J. Electrochem. Solid-State Lett. 9 (2006) A110.
[22] C. Wang, I. Kakwan, A.J. Appleby, F.E. Little, J. Electroanal. Chem. 489 (2000) 55.
[23] McC. Siebert, W. Circuits, Signals and System, The MIT Press and McGraw-Hill Book Company, New York, 1986.